Research Paper

Ringing Detector for Deblurring
based on Frequency Analysis of PSF

Chika Inoshita,[†1] Yasuhiro Mukaigawa[†1]
and Yasushi Yagi[†1]

Many deblurring techniques have been proposed to restore blurred images resulting from camera motion. A major problem in the restoration process is that the deblurred images often include wave-like artifacts called ringing. In this paper, we propose a ringing detector that distinguishes the ringing artifacts from natural textures included in images. In designing the ringing detector, we focus on the fact that ringing artifacts are caused by the null frequency of the point-spread function. Ringings are detected by evaluating whether the deblurred image contains sine waves corresponding to the null frequencies across the entire image with uniform phase. By combining the ringing detector with a deblurring process, we can reduce ringing artifacts in the restored images. We demonstrate the effectiveness of the proposed ringing detector in experiments with synthetic and real images.

1. Introduction

Images are blurred by the camera or object motion during exposure. Despite the inclusion of a vibration reduction function or highly sensitive imaging devices in the latest conventional cameras to reduce the effect of motion, blurring cannot be solved by camera settings alone. Hence, restoration through image processing is frequently required. However, it is very difficult to restore the blurred image when its blur kernel is unknown [1]. In theory, images can be deblurred if the blur kernels of the camera or object motion are known. However, blurred images cannot be completely even with the known blur kernel for various reasons, including image noise and calculation error. As a result, deblurred images often include wave-like artifacts known as ringing.

In previous studies on image deblurring, many researchers have tried reducing ringing in deblurred images. Shan et al. [2] evaluated smoothness in a textureless area to reduce ringing. Yuan et al. [3] proposed a restoration technique using the residual image in which the ringing amplitude is proportional to the amplitude of the edges in the image. Almost all current deblurring methods use statistical or empirical features of ringing, and therefore do not strictly address the reason why ringing occurs. In fact, it is difficult to detect the ringing from the deblurred image alone.

In previous studies, ringing artifacts have been analyzed in detail. Lagendijk et al. [4] analyzed ringing effects caused by the linear space-invariant image restoration. They treated ringing specifically as restoration error such as noise and regularization, however physical characteristics of ringing were not considered. Several ringing detectors have been proposed to determine image quality. Nasonov and Krylov [5] proposed an estimation algorithm based on total variation control. Zuo et al. [6],[7] evaluated ringing artifacts using a Gabor filter. Although these methods can detect ringing, the detectors sometimes react to edges or periodic structures that are not ringing artifacts, since the methods do not consider the frequency, direction, or spatial characteristics of the ringing.

In this paper, we propose a novel ringing detector that distinguishes ringing artifacts from natural wave-like textures in images. To design the ringing detector, we determine frequencies for the ringing and detect the ringing features based on a frequency analysis of the point-spread function (PSF). Using the ringing detector, it is possible to focus exclusively on the frequencies of the ringing. Moreover, we demonstrate that the ringing detector can be used for image deblurring without affecting the texture of the original image.

Contribution

The contributions of this work are as follows.

- We identify the features of ringing based on a frequency analysis of the PSF. Our approach focuses on the physical features of ringing artifacts, and not on statistical or empirical features.
- We have designed a novel ringing detector that clearly distinguishes ringing artifacts from natural textures included in images.
- Our ringing detector can be combined with usual deblurring techniques as a part of the energy function. The combination enables us to reduce ringing

---

†1 Institute of Scientific and Industrial Research, Osaka University

artifacts in deblurred images.

2. Related Work

Statistical or empirical features of images: It is known that the gradient histogram of a natural image has a heavy-tailed distribution. Shan et al. [2] approximated this distribution using a polynomial function and applied it to the maximum a posteriori (MAP) estimation. Fergus et al. [8] adopted this feature in a Bayesian approach [9]. On the other hand, since the amplitude of ringing is proportional to the amplitude of the edges in an image, several methods using the residual image have also been proposed [3],[10]. In these methods, ringing resulting from the deblurring process cannot be distinguished from the wave-like textures in images, because these methods are unable to separate the ringing frequencies from other frequencies. Since our approach is based on a physical frequency analysis, it can identify the frequency of the ringing, and is thus able to distinguish ringing artifacts from wave-like textures.

Using multiple images: If the PSF is unknown, restoration is difficult using only the blurred image. Hence, restoration methods using multiple images have been proposed. Ancuti et al. [11] estimated the PSF of a blurred image by combining a non-blurred image that includes the same object that is to be restored in the blurred image. Rav-Acha and Peleg [12] proposed a dual-kernel estimation algorithm that uses two blurred images, and the algorithm was later improved by Chen et al. [13]. Ben-Ezra and Nayar [14] used a hybrid camera that combines a low-resolution video camera for estimating the PSF and a high-resolution still camera. Tai et al. [15] also used a hybrid camera. However, they used low-resolution video images for estimating spatially varying PSF by optical flow.

L1-norm-based regularization: Regularization-based image deconvolution is widely employed. In particular, L1-norm-based regularization is effective for precise image restoration. Various methods have been proposed for L1 norm evaluation such as total variation (TV) regularization [23]–[25], sparse regularization [26], and wavelet regularization [27]. These methods can restore blurred images accurately; however, these methods often contain errors because the approach does not consider physical features.

Computational photography: In the field of computational photography,

ringing is prevented by means of photographic techniques. A camera with an encoded close-and-open shutter operation is used to reduce the effect of lost frequency components [16]–[18]. Although these techniques can restore blurred images accurately, they cannot be applied to images taken with a normal camera. Agrawal et al. [19] used multiple images taken with different exposures. Since the frequency components of captured images complement each lost frequency component, deblurred image restoration can be solved as a well posed problem. However, this approach requires multiple images for restoration. Our method, on the other hand, requires neither special camera settings nor multiple images.

Cepstrum: The cepstrum is defined as the logarithm of the frequency power spectrum. As seen later in this paper, a blurred image is modeled by the convolution of the original image and the PSF, while the frequency power spectrum of the blurred image is similar to that of the PSF. As a result, the cepstrum of the blurred image has characteristics similar to that of the PSFs. Thus, the cepstrum is used to estimate the PSF [20]–[22]. This method and our approach are based on the same frequency analysis, however, the purpose of our method is different from theirs. Whereas their method uses frequency analysis to estimate the PSF, we use it for detecting ringing.

3. Ringing Detector

3.1 Principle of Blurred Image Restoration

First, we summarize the principle of deblurring based on a Fourier transformation when the PSF is known. If the blur kernel on the blurred image is uniform, the blurred image l can be modeled by the convolution of the image f and the PSF b as

$$l = f * b, \tag{1}$$

where '$*$' denotes the convolution. In the frequency domain, the convolution is represented by multiplication. Therefore, Eq. (1) is transformed using the Fourier transformation given below.

$$\mathcal{F}(l) = \mathcal{F}(f)\mathcal{F}(b), \tag{2}$$

where $\mathcal{F}()$ represents the Fourier transformation. The blurred image is restored by the inverse Fourier transformation of the blurred image divided at each element by the PSF in the frequency domain as
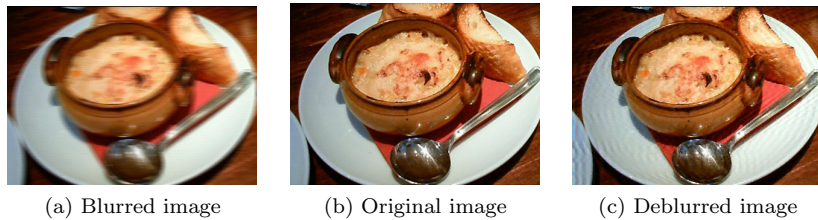
(a) Blurred image   (b) Original image   (c) Deblurred image

Fig. 1 An example of image restoration. The deblurred image has wave-like artifacts.

$$r = \mathcal{F}^{-1}\left(\frac{\mathcal{F}(l)}{\mathcal{F}(b)}\right), \tag{3}$$

where $\mathcal{F}^{-1}()$ represents the inverse Fourier transformation, and r represents the deblurred image. This is the principle of deblurring when the PSF is known.

3.2 Ringing Resulting from Deblurring

In theory, it is possible to restore blurred images on the basis of Fourier transformation as described in Section 3.1. However, we cannot completely restore blurred images for a variety of reasons. **Figure 1** shows an example of a deblurred image. The deblurred image in Fig. 1 (c) has wave-like artifacts, which are not present in the original image. The main reason is that the blurred image loses its specific frequency component. We call this lost frequency the *null frequency*.

The wave-like artifacts are caused by the null frequency of the PSF. The blurred image modeled by Eq. (2) loses frequency components corresponding to the null frequencies of the PSF. Since division of a small value by a similar small value tends to be unstable, the frequency components of the blurred image are not correctly restored. We call a frequency causing a large error a *noninvertible frequency*.

Figure 2 illustrates blur restoration using a one-dimensional (1-D) signal. Since the PSF in Fig. 2 has two null frequencies, the deblurred signal has large values corresponding to the noninvertible frequencies. As seen in Fig. 2, the deblurred signal is incorrectly restored at the noninvertible frequency. Thus, the deblurred signal includes sine waves with uniform phases corresponding to the null frequencies across the entire signal. These sine waves are components of ringing.
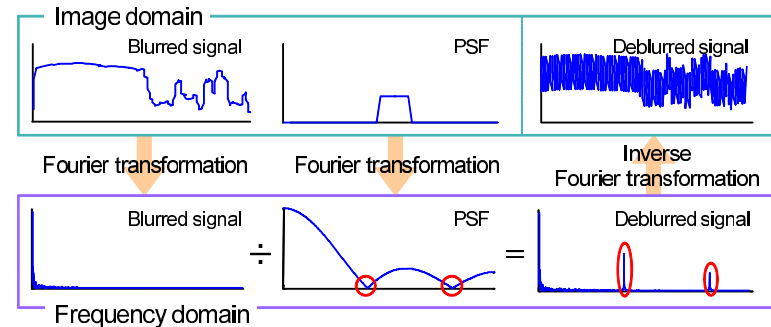

Fig. 2 Deblurring for a 1-D signal. The PSF has null frequencies denoted by red circles. The deblurred signal has incorrect frequency spectrums denoted by red ellipses.

Although several researchers have discussed various forms of ringing, we focus on ringing caused by null frequencies of the PSF in this paper.

3.3 Model of Ringing

If the PSF is known, the frequency and direction of the sine waves comprising the ringing (referred to as *error waves*) can be accurately predicted from the frequency components of the PSF. In addition, since error waves appear in the entire image with uniform phase, the deblurred image $r(x,y)$ with ringing artifacts is expressed as the sum of the original image $f(x,y)$ and the error waves $e_i(x,y)$ as

$$r(x,y) = f(x,y) + \sum_i e_i(x,y). \tag{4}$$

Error waves are sine waves corresponding to the noninvertible frequencies as

$$e_i(x,y) = k_i \cos(2\pi(a_i x + b_i y) + c_i), \tag{5}$$

where a_i and b_i are the x- and y-axis frequencies, respectively, corresponding to the noninvertible frequencies of the PSF, k_i is the unknown amplitude, and c_i is the unknown phase. A deblurred image with reduced ringing can be obtained by removing the error waves from the deblurred image.

3.4 Design of a Ringing Detector
3.4.1 Features of Ringing

We explained the cause of ringing in the preceding section. Although ringing is expressed by the sum of error waves as shown in Eq. (4), it is difficult to

(a) Ringing textures in deblurred image　　　(b) Wave-like textures in natural image
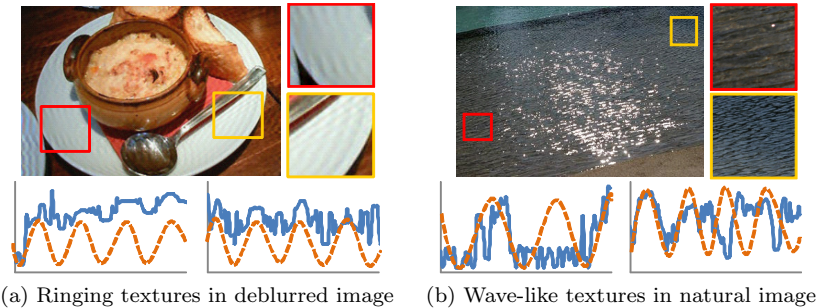
Fig. 3　Examples of wave textures. Each instance shows the full-size image, the clipped images, and the intensity profiles of the clipped images. The orange broken lines depict sine waves. (a) A deblurred image has ringing textures with uniform phase, direction and frequency. The broken line, which is a sine wave with uniform phase, matches the horizontal brightness profile. (b) A natural image has wave textures with varying directions, phases, and frequencies. Thus, a sine wave with uniform phase is not observed in the graph.

determine from the deblurring result alone whether ringing exists. Since some images consist of various sine waves such as the example in **Fig. 3** (b), we cannot distinguish the ringing artifacts from the natural textures in those images. Thus, we need to analyze the characteristics of the physical features of ringing.

Figure 3 shows examples of wave-like textures in a variety of images. Each example shows the original image, clipped images, and graphs showing the horizontal intensity profile of the clipped images. Figure 3 (a) illustrates the deblurred image, which has wave-like textures across the entire image resulting from the ringing. Both graphs in Fig. 3 (a) show that the horizontal intensity can be expressed as a sine wave with uniform phase depicted by the orange broken line. On the other hand, Fig. 3 (b) shows a natural image with wave-like textures. It should be noted that, although we can observe a sine wave in the graphs in Fig. 3 (b), the phase thereof is not uniform.

The intensity profile of the natural image of Fig. 3 (b) does not have a sine wave with uniform phase. In fact the orange broken line indicating a sine wave does not correlate with the intensity profiles. Instead, natural images consist of sine waves with varying frequencies, directions, and phases. Thus, it is rare that specific sine waves with uniform phase are included in the images.

As explained above, it is clear that ringing is included in deblurred images as a sine wave with uniform phase. In addition, we explained that the ringing consists of a sine wave with frequency equal to the noninvertible frequency of the PSF in Section 3.3. Features of the error waves comprising the ringing artifacts are summarized as follows.

(1)　A frequency and direction correspond to the noninvertible frequency of the PSF.

(2)　Phases of error waves are uniform in a deblurred image.

The noninvertible frequencies are decided by the PSF's frequency components that have little power. However, it is necessary to analyze whether the phase of the error waves is uniform or not. The ringing detector examines this feature.

Since images consist of sine waves with various frequencies and phases, we need to extract the error wave before examining the phase condition. The ringing detector executes the following two steps.

(a)　Extraction of the error wave

(b)　Examination of the phase condition

Each step is described in detail in the following sections.

3.4.2　Extraction of the Error Wave

The Gabor transformation analyzes local frequency characteristics, and is expressed by the convolution as

$$g_i(x,y) = \sum_{s,t} r(x-s, y-t) w_i(s,t), \tag{6}$$

$$w_i(x,y) = \frac{1}{2\pi d^2} e^{-\frac{x^2+y^2}{2d^2}} \cos(2\pi(a_i x + b_i y)), \tag{7}$$

where $w_i()$ is the Gabor filter, d is the variance, a_i is the x-axis frequency, and b_i is the y-axis frequency. a_i and b_i are determined according to the noninvertible frequencies. Inputs to the ringing detector are these frequencies and the deblurred image $r(x,y)$. If the sine wave corresponding to the input frequency is included in the input image with uniform phase, the Gabor transformation result almost matches the sine wave with the given frequency and uniform phase.

Figure 4 illustrates examples of the Gabor transformation results of a 1-D signal with and without error waves. The Gabor transformation results represent the behavior of the frequency component that is assigned to the Gabor filter.

3.4.3   Examination of the Phase Condition

After the Gabor transformation, we examine whether the phase of the error wave is uniform or not. If ringing has occurred, the Gabor transformation result has a periodic pattern that corresponds to the input frequency. Thus, we use the correlation coefficient between the Gabor transformation result and the error wave to examine whether the transformation result has uniform phase. However, the phase c_i and amplitude k_i of the error wave $e_i(x, y)$ are unknown. Therefore, k_i is fixed to 1 and c_i is estimated by seeking the phase that maximizes the correlation coefficient $C_i(c)$. The ringing detector outputs the maximum value of $C_i(c)$, in the range 0 to 1. If the output is close to 1, the phases are uniform in different areas. Thus, whether the sine wave in an image has a uniform phase is ascertained from the output of the ringing detector.

Figure 4 illustrates that if error waves are included in the signal, the frequency and phase of the Gabor transformation result almost match those of the error waves. In contrast, if error waves are not included in the signal, the frequency and phase of the transformation result have no correlation with those of the error
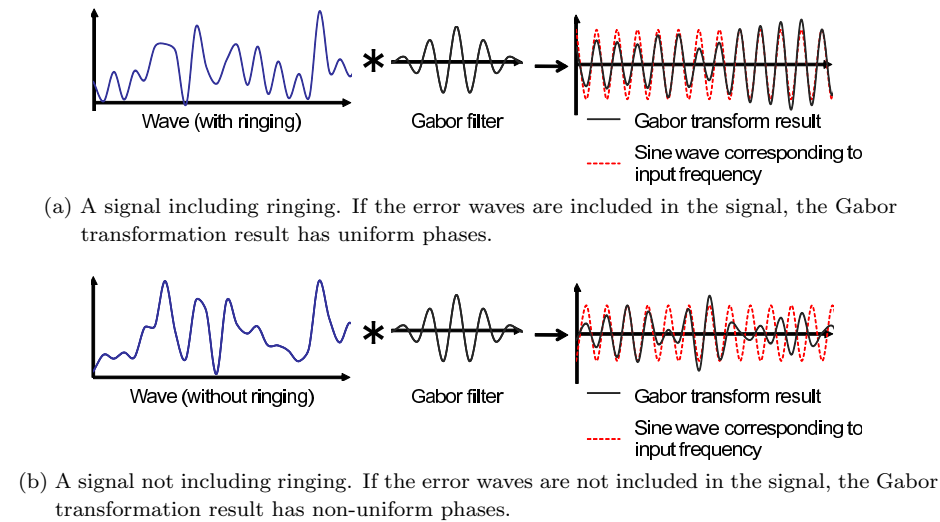
waves. Thus, the error wave overlaps the Gabor transformation result as shown in Fig. 4 (a), and the output of the ringing detector is close to 1.

4.   Experimental Results

4.1   Validation of the Ringing Detector

First, we confirmed whether the ringing detector reacts to ringing artifacts. We evaluated the output of the ringing detector using synthetic images based on Eq. (4). The image used in the experiment is shown in Fig. 3 (a). In the experiment, k_i in Eq. (4) was varied between -1 and 1 in 0.1 steps, while a_i and b_i were varied between -0.4 and 0.4 in 0.1 steps. We input $r(x, y)$ in Eq. (4) and a_i and b_i in Eq. (5) into the ringing detector, and examined the output value. Since k_i represents the amplitude of ringing, we would expect the output of the ringing detector to yield a minimum value as k_i approaches zero.

Figure 5 (a) and (b) show the experimental results. The horizontal axis represents the ringing amplitude k_i, while the vertical axis represents the output of the ringing detector. For all b_i, the ringing detector outputs the minimum value when the ringing amplitude is close to zero. In addition, the value of 1 for k_i is unperceivable in 8-bit format. Human eyes cannot distinguish the slight difference. Although the ringing amplitude is slight, a certain amount of output
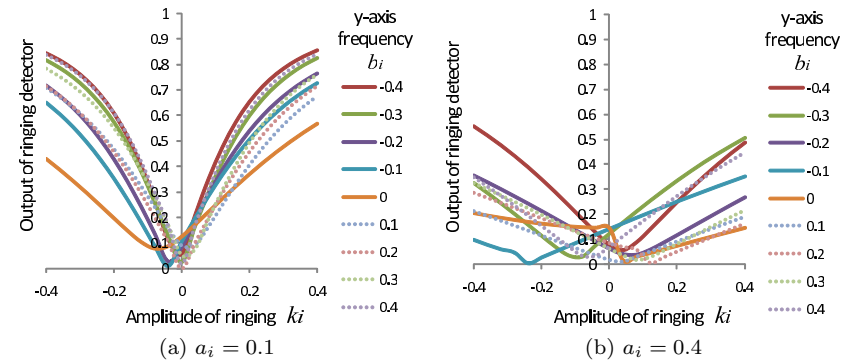
(a) A signal including ringing. If the error waves are included in the signal, the Gabor transformation result has uniform phases.

(b) A signal not including ringing. If the error waves are not included in the signal, the Gabor transformation result has non-uniform phases.

Fig. 4   Examples of Gabor transformation.

(a) $a_i = 0.1$ (b) $a_i = 0.4$

Fig. 5   Outputs of the ringing detector. Both (a) and (b) have minimum output values for x-axis values close to zero. We see that the ringing detector reacts to slight ringing artifacts and does not react to natural textures.

(a) $a = 0.125$, $b = 0.125$ (b) $a = 0.25$, $b = 0$
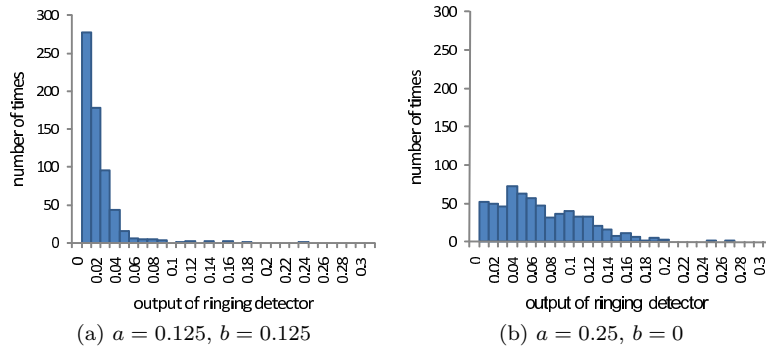
Fig. 6 Histogram of ringing detector outputs. Since almost all outputs have small values, we see that the ringing detector does not react to natural textures.

Table 1 Maximum output values of the ringing detector with various x- and y-axis frequencies. Almost output values are less than 0.25. Since almost all output values are small, the ringing detector does not react to natural textures.

		x-axis frequency a				
		0	0.1	0.125	0.2	0.25
	0.000	−	0.16	0.19	0.21	0.26
	0.100	0.23	0.07	0.09	0.09	0.10
y-axis frequency b	0.125	0.34	0.10	0.23	0.11	0.22
	0.20	0.23	0.07	0.09	0.06	0.10
	0.250	0.27	0.10	0.23	0.10	0.07

is obtained when the absolute value of the horizontal axis is 0.4. Therefore, we can confirm that the ringing detector reacts if the image includes ringing, and does not react if the image does not include ringing.

4.2 Feature Analysis of Texture Contained in a Natural Image

Having confirmed that the ringing detector does not react to textures in natural images, we then applied the ringing detector to a variety of images with various frequencies, and observed the output values. The frequencies in Eq. (7) are all combinations of the x-axis frequency a_i and y-axis frequency b_i being set to $0, 0.1, 0.125, 0.2, 0.25$ except when $a_i = b_i = 0$, as this implies no ringing. Here, frequency is the inverse pixel number of the sine wave period. The data sets are 600 images downloaded from flickr[*1] using various keywords such as scene, flower, animal, building, and human.

Figure 6 (a) shows the histogram of the ringing detector outputs for the input images with x-axis frequency $a_i = 0.125$ and y-axis frequency $b_i = 0.125$. The ringing detector outputs small values for most input images. Figure 6 (b) shows the histogram with the x-axis frequency $a_i = 0.25$ and the y-axis frequency $b_i = 0$. Most outputs are less than 0.2.

Maximum output values of the ringing detector are shown in **Table 1**. Ac-

cording to the table, it is clear that the ringing detector does not react to the textures in natural images.

5. Application to Deblurring

5.1 Deblurring Using the Ringing Detector

A deblurred image based on the inverse Fourier transformation is the sum of the original image and the error waves as expressed by Eq. (4). The frequencies and directions of the error waves can be specified by frequency analysis of the PSF. That is, we can reduce the ringing in a deblurred image by finding values for the ringing amplitude and phase that minimize the output of the ringing detector. However, the detector needs to know the noninvertible frequencies of the PSF, since this deblurring method can be applied only when the PSF is known or can be accurately estimated.

Figure 7 shows the restoration process flow using the ringing detector.

(1) Restore blurred image through inverse Fourier transformation as Eq. (3).

(2) Search for the noninvertible frequency with a small power value in the frequency domain of the PSF.

(3) Input the deblurred image and noninvertible frequency to the ringing detector. If the output is smaller than a threshold, return to step 2.

(4) Reduce the ringing from the deblurred image. Firstly, phase c_i of the error wave is estimated. When the phases of the error wave and ringing correspond, the ringing detector outputs a maximum value. Hence, the phase c_i that maximizes the output of the ringing detector $C_i(c)$ is found by shifting the phase from 0 to 2π. Next, the ringing is reduced. We assume
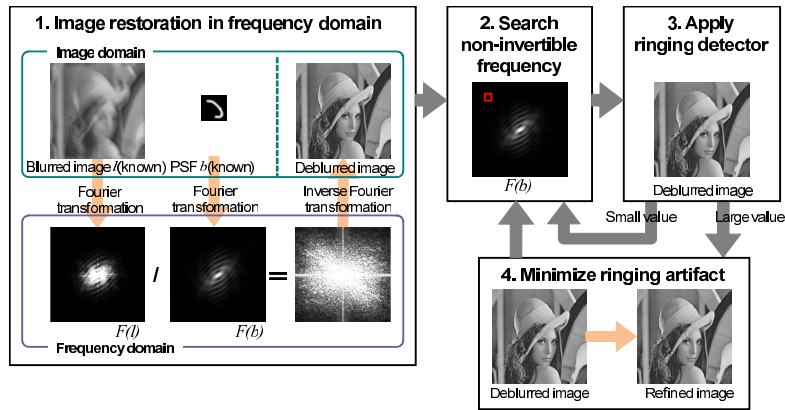

[*1] http://www.flickr.com/

Fig. 7 Process flow to restore a blurred image using a ringing detector.

(a) building   (b) desk   (c) road

Fig. 8 Images used in the restoration experiment.

(a) PSF1   (b) PSF1 in frequency domain   (c) Noninvertible frequencies of PSF1

(d) PSF2   (e) PSF2 in frequency domain   (f) Noninvertible frequencies of PSF2
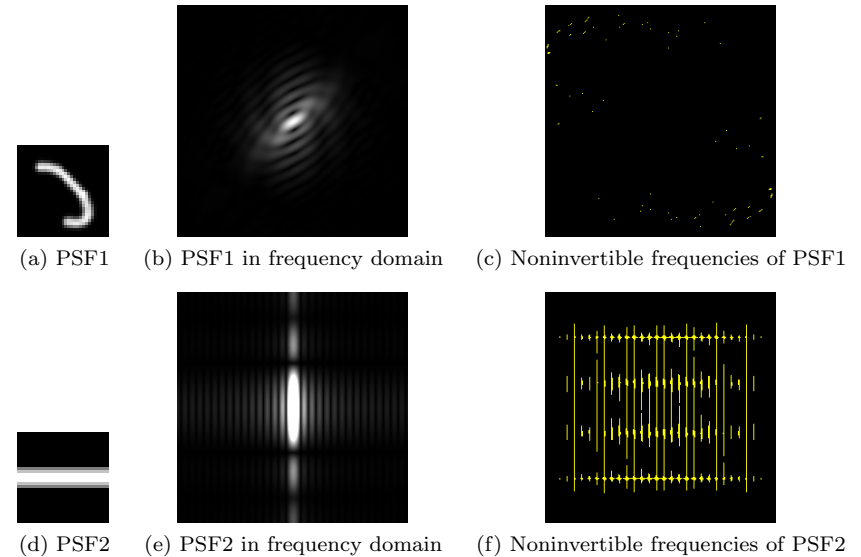
Fig. 9 PSFs for the restoration experiment. Yellow points in (c) and (f) show noninvertible frequencies.

that the output of the ringing detector approaches zero when the ringing is reduced. Hence, the amplitude k_i that minimizes the output of the ringing detector $C_i(c)$ is found by changing the amplitude. The estimated c_i and k_i determine the error wave included in the deblurred image. By subtracting the error wave from the deblurred image, the ringing is reduced. Repeat steps from 2 to 4 until the search for the noninvertible frequency is complete.

5.2 Restoration of Synthetic Images

We demonstrate that a deblurred image can be improved using the ringing detector. The blurred images for the experiment were synthesized from original images as shown in **Fig. 8** and known PSFs as shown in **Fig. 9** (a) and (d). Figure 9 (b) and (e) show the PSFs in the frequency domain, and Fig. 9 (c) and (f) indicate the noninvertible frequencies with yellow points. We used the peak signal-to-noise ratio (PSNR) to evaluate the restoration results. To confirm the effectiveness of our approach, we compared it with several other restoration methods including inverse Fourier transformation as in Eq. (3), Richardson-Lucy deconvolution [28], the Wiener filter [29], the method of Shan et al. [2], TV regularization [25] and wavelet regularization [27]. It is noted that all these restoration methods other than that of Shan et al. [2] are non-blind deconvolution. For all non-blind methods, we gave an accurate PSF.
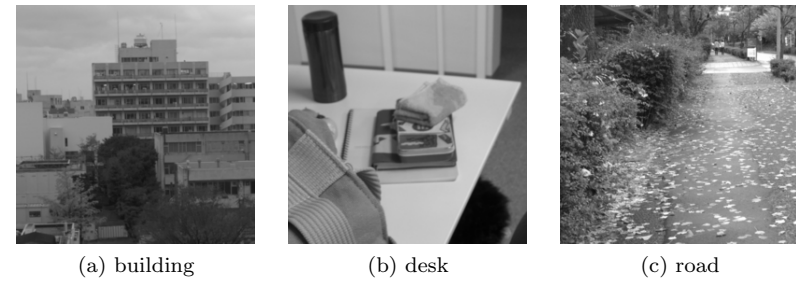
Table 2 and **Table 3** present the PSNRs between the original image and the restoration images. We see that the PSNR of our method is highest for all experiments. **Figure 10** shows the clipped restoration image for Fig. 8 (a).

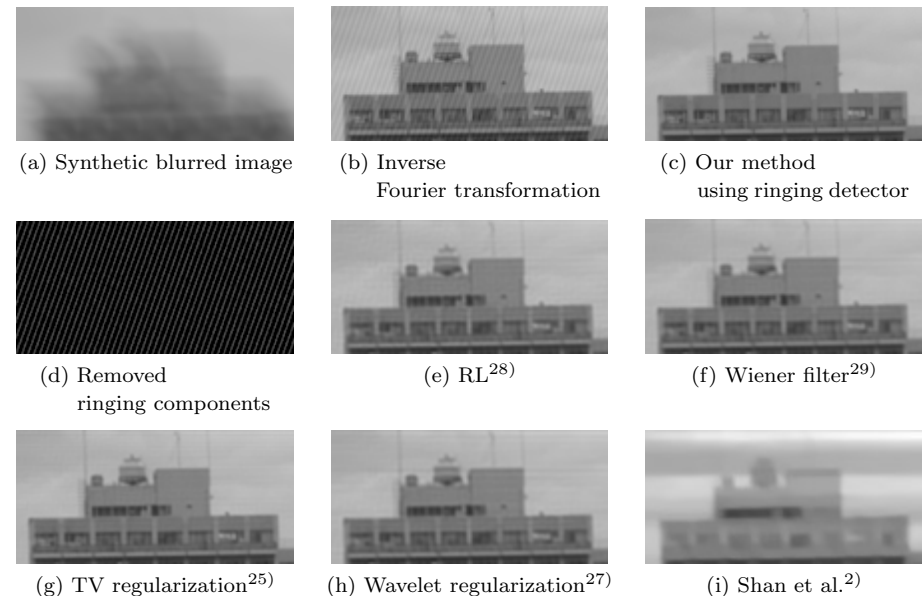**Table 2**   PSNR (dB) of restoration results obtained using PSF1. Our method yields the highest PSNR.

	building	desk	road
Our method using ringing detector	53.62	54.07	53.62
Inverse Fourier transformation	35.16	41.73	35.38
Richardson-Lucy	37.62	39.2	32.05
Wiener filter	37.75	40.73	37.21
Shan et al. [2]	21.17	20.32	19.78
TV regularization [25]	42.34	45.09	36.33
Wavelet regularization [27]	36.86	39.83	31.34

Table 3   PSNR (dB) of restoration results obtained using PSF2.

	building	desk	road
Our method using ringing detector	45.29	46.13	44.07
Inverse Fourier transformation	42.48	42.52	40.89
Richardson-Lucy	37.67	36.55	29.32
Wiener filter	38.06	37.62	33.25
Shan et al. [2]	21.88	21.44	19.53
TV regularization [25]	42.38	42.87	33.42
Wavelet regularization [27]	37.99	37.27	29.17

(a) Synthetic blurred image   (b) Inverse Fourier transformation   (c) Our method using ringing detector

(d) Removed ringing components   (e) RL[28]   (f) Wiener filter[29]

(g) TV regularization[25]   (h) Wavelet regularization[27]   (i) Shan et al.[2]

Fig. 10   Clipped restored images. Wave-like textures are observed in (b), but they are reduced in (c). Removed ringing components are shown in (d).

Although Fig. 10 (b) includes a wave-like diagonal texture, it has been reduced in the restoration image obtained using our method as seen in Fig. 10 (c). Figure 10 (d) shows the removed ringing components. This component corresponds to the diagonal texture in Fig. 10 (b). We can say that our method achieves better restoration than other deblurring methods.

In this experiment, PSNRs achieved by the simple inverse Fourier transformation were sometimes larger than those achieved by regularization-based methods. We believe that these unusual results were due to an absence of noise. While synthetic images are blurred, they do not include noise. This condition is advantageous for simple deconvolution. On the other hand, regularization included in RL and the method of Shan et al. affects the restoration result.

5.3   Restoration of Real Images

Finally, we present deblurring results for a real image. We captured a blurred image using a Nikon D80 camera by fixing the camera on a tripod and rotating it around the optical axis without horizontal or vertical rotation of the camera. The camera function of optical vibration reduction was not used, the shutter speed was set to 0.1 s, and the gamma value was set to 1 to make the response function linear.

Figure 11 shows the captured image. We estimated several PSFs by tracking point light sources placed on both sides of the target object (**Fig. 12**), and selected the one that restored the best result. **Figure 13** shows the estimated PSF. Figure 13 compares restoration results obtained using several methods. (b) is the inverse Fourier transformation, (c) is the result obtained using our approach, (e) is the TV regularization [25], (f) is the wavelet regularization [27] and

Fig. 11 Captured real image. Point light sources were placed on either side of the subject to estimate the PSF.
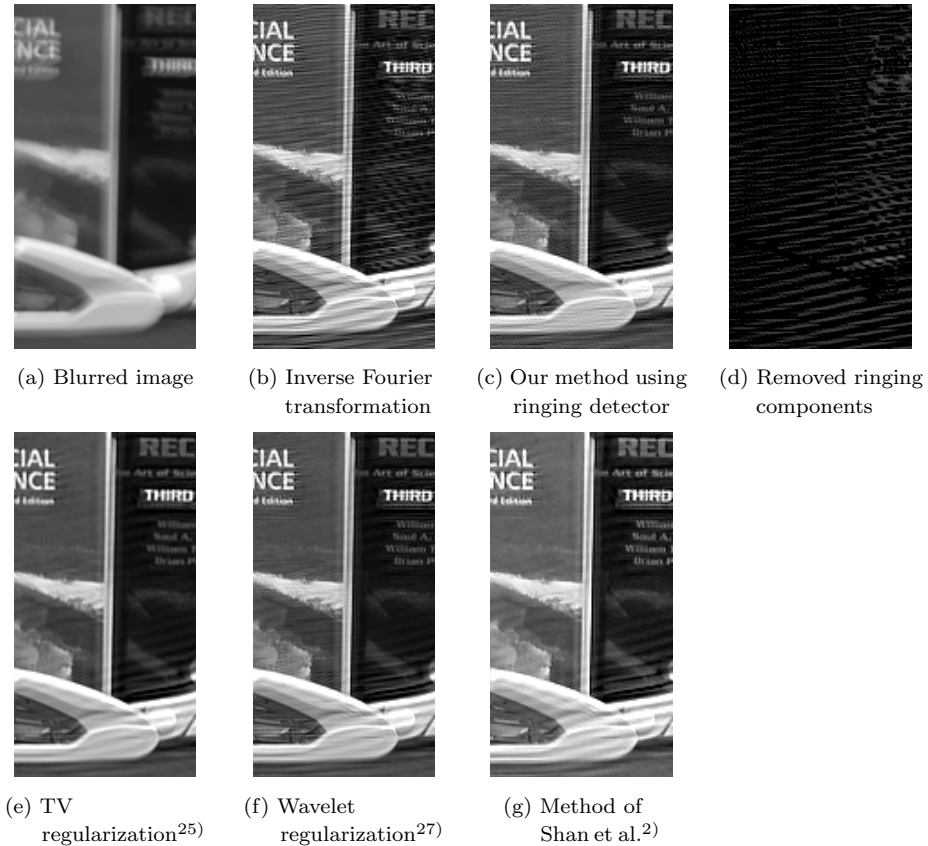

(a) Left

(b) Right

Fig. 12 Trajectories of a point light source. These results were used to estimate the PSF.

(a) Blurred image

(b) Inverse Fourier transformation

(c) Our method using ringing detector

(d) Removed ringing components

(e) TV regularization[25]

(f) Wavelet regularization[27]

(g) Method of Shan et al.[2]

Fig. 13 Experimental results obtained using a real blurred image. (a) is the blurred image, (b) is the inverse Fourier transformation, (c) is the result obtained using our method, (d) is removed ringing components with our method, (e) is TV regularization, (f) is wavelet transformation, and (g) is the result obtained using the method of Shan et al. Although the ringing artifacts are not reduced completely, (c) shows clearer book textures than (b). Other restoration results also have the ringing effect.

(g) is the result of using the method of Shan et al.[2]. Figure 13 (b) $\sim$ (e) have sharper edges compared with (a), since these are deblurred. In addition, ringing artifacts in (c) are reduced compared with those in (b). We show the removed ringing component in Fig. 13 (d). Figure 13 (c) has reduced ringing artifacts on the scissors compared with other results. However, the ringing artifacts are not completely removed in any of the restoration results. This may be the result of an incorrectly estimated PSF.

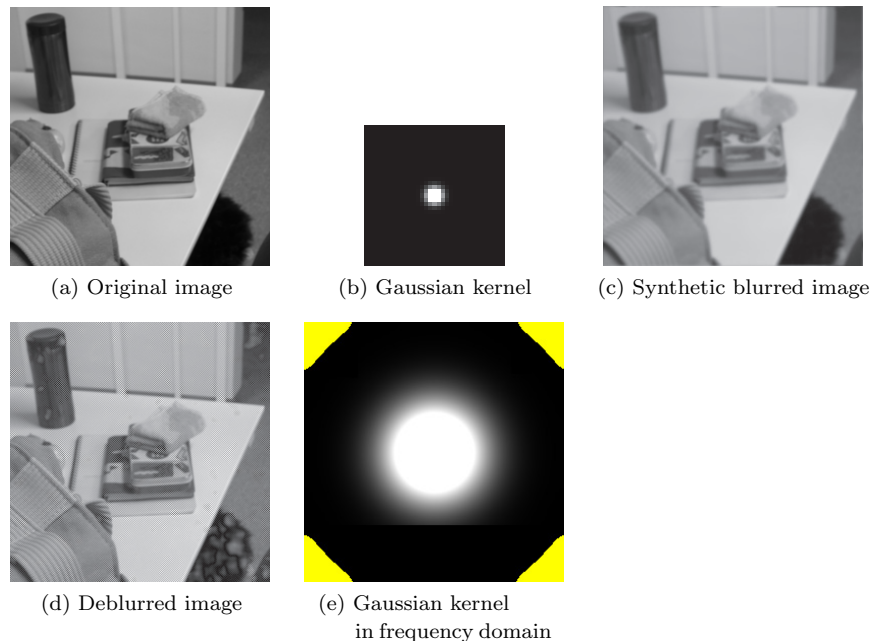### 5.4 Application of the Defocusing Problem

In this paper, we focused only on motion blur. Although defocus blur and motion blur are similar because both are modeled as a convolution with the blur kernel, their characteristics of noninvertible frequency are different. The motion blur has specific noninvertible frequencies, while the defocus blur has an area of noninvertible frequencies. Therefore, it is difficult to apply our restoration method for the defocus blur because these are too many noninvertible frequencies.

Figure 14 shows an example of defocus blur. Figure 14 (a) is an original image and the same as Fig. 9 (b), and (b) is the PSF of the Gaussian blur kernel. (c) is a blurred image synthesized by convolution of (a) and (b). (d) is the result of simple deconvolution by inverse Fourier transformation. Many artifacts are observed. (e) shows the PSF in the frequency domain. Many noninvertible frequencies,

which are indicated by yellow points, exist. Hence, we know that the deblurred image includes ringing artifacts, which are difficult to reduce.

(a) Original image   (b) Gaussian kernel   (c) Synthetic blurred image

(d) Deblurred image   (e) Gaussian kernel
in frequency domain

Fig. 14 Application to a deblurring problem. (a) is the original image, (b) is the Gaussian blur kernel, and (c) is the synthetic image blurred by the convolution of (a) and (b). (d) is simple deconvolution, or which there are many artifacts. (e) is the Gaussian kernel in the frequency domain. The ringing detector can detect ringing in (d); however, it is difficult to reduce artifacts because of the many noninvertible frequencies.

6. Limitations

The limitations of the approach proposed in this paper are as follows.

- Since we analyze the null frequencies of the PSF for the ringing detector, the PSF must be known.
- We cannot completely restore the blurred image if the given PSF has errors. Since our approach deals only with the noninvertible frequencies of the PSF, we cannot restore the other frequencies.
- Since we ignored the noise problem, we cannot reduce the ringing due to noise. If the blurred image includes noise, the restoration result degrades.

- We cannot recover the power of the noninvertible frequencies directly using a ringing detector. The ringing detector only evaluates whether the features of ringing are satisfied. Thus, in the process of reducing ringing artifacts, much time is needed to compute the ringing amplitude.
- If natural images coincidentally include sine wave textures corresponding to the noninvertible frequencies with uniform phases, the ringing detector will react to these textures.
- In this paper, we assume that the blur kernel in the blurred image is entirely uniform. Thus, we cannot apply the ringing detector to a blurred image with spatially varying blur kernels.
- We cannot completely remove other ringing artifacts such as boundary ringing or edge ringing. Because we focused only on the ringing artifact which is included in blurred image entirely with uniform phase.

7. Conclusions and Discussion

In this paper, we proposed a ringing detector to distinguish ringing artifacts from natural textures. Because the design of the ringing detector is based on a frequency analysis of the PSF, we can focus independently on the frequencies of the ringing. We confirmed the performance of the ringing detector in experiments. Moreover, we modeled deblurred images as the sum of the original image and the error waves, and proposed using the ringing detector for deblurring.

In this paper, we ignored image noise and focused only on the ringing artifacts that arise even if images do not include noise. Noise also causes different types of ringing problems that do not occur in the invertible Fourier transformation of the PSF. As an extension, we need to consider the noise effect in the ringing reduction.

Moreover, we assume that the PSF is uniform across the entire image. However, real blurs are often nonuniform. Some techniques have been proposed to handle blurs resulting from general motions such as object motion [30], camera shake [31],[32], non-uniform motion which is combined with some uniform blurred regions [33]. To handle spatially varying PSF, inertial sensors are used [34]. We intend to apply our ringing detector to more general blurred images by dividing images to several subregions in which the PSF can be assumed as uniform. Fur-

thermore, we aim to develop a new restoration method by combining our ringing detector with state-of-the-art deblurring techniques.

References

1) Levin, A., Weiss, Y., Durand, F. and Freeman, W.T.: Understanding and evaluating blind deconvolution algorithms, *IEEE Conference on Computer Vision Pattern Recognition* (2009).
2) Shan, Q., Jia, J. and Agarwal, A.: High-quality motion deblurring from a single image, *ACM Trans. Gr.*, Vol.27, No.3, pp.73:1–73:10 (2008).
3) Yuan, L., Sun, J., Quan, L. and Shum, H.-Y.: Image deblurring with blurred/noisy image pairs, *ACM Trans. Gr.*, Vol.26, No.3, p.1 (2007).
4) Lagendijk, R.L., Biemond, J. and Boekee, D.E.: Regularized iterative image restoration with ringing reduction, *IEEE Trans. Acoustics, Speech and Signal Processing*, Vol.36, No.12, pp.1874–1888 (1988).
5) Nasonov, A.V. and Krylov, A.S.: Scale-space method of image ringing estimation, *International Conference on Image Processing*, pp.2794–2797 (2009).
6) Zuo, B.-X., Tian, J.-W. and Ming, D.-L.: A no-reference ringing metric for images deconvolution, *Wavelet Analysis and Pattern Recognition*, Vol.1, pp.96–101 (2008).
7) Zuo, B.-X.: Perceptual ringing metric to evaluate the quality of images restored using blind deconvolution algorithms, *Optical Engineering*, Vol.48, No.3, p.037004 (2009).
8) Fergus, R., Singh, B., Herzmann, A., Roweis, S.T. and Freeman, W.T.: Removing camera shake from a single photograph, *ACM Trans. Gr.*, Vol.25, No.3, pp.787–794 (2006).
9) Miskin, J. and MacKay, D.J.C.: Ensemble learning for blind image separation and deconvolution, *Advances in Independent Component Analysis*, Springer-Verlag (2000).
10) Yuan, L., Sun, J., Quan, L. and Shum, H.-Y.: Progressive inter-scale and intra-scale non-blind image deconvolution, *ACM Trans. Gr.*, Vol.27, No.3, pp.74:1–74:10 (2008).
11) Ancuti, C., Ancuti, C.O. and Bekaert, P.: Deblurring by Matching, *Computer Graphics Forum*, Vol.28, No.2, pp.619–628 (2009).
12) Rav-Acha, A. and Peleg, S.: Two motion blurred images are better than one, *Pattern Recognition Letters*, No.26, pp.311–317 (2005).
13) Chen, J., Yuan, L., Tang, C.K. and Quan, K.: Robust dual motion deblurring, *IEEE Conference on Computer Vision Pattern Recognition* (2008).
14) Ben-Ezra, M. and Nayar, S.K.: Motion-Based Motion Deblurring, *IEEE Trans. Pattern Analysis and Machine Intelligence*, Vol.26, No.6, pp.689–698 (2004).
15) Tai, Y.-W., Du, H., Brown, M.S. and Lin, S.: Correction of Spatially Varying Image and Video Motion Blur using a Hybrid Camera, *IEEE TPAMI*, Vol.32, No.6, pp.1012–1028 (2010).
16) Raskar, R., Agrawal, A. and Tumblin, J.: Coded exposure photography: Motion deblurring using fluttered shutter, *ACM Trans. Gr.*, Vol.25, No.3, pp.795–804 (2006).
17) Agrawal, A. and Xu, Y.: Coded exposure deblurring: Optimized codes for PSF estimation and invertibility, *IEEE Conference on Computer Vision and Pattern Recognition* (2009).
18) Tai, Y., Kong, N., Lin, S. and Shin, S.Y.: Coded exposure imaging for projective motion deblurring, *IEEE Conference on Computer Vision and Pattern Recognition* (2010).
19) Agrawal, A., Xu, Y. and Raskar, R.: Invertible motion blur in a video, *ACM Trans. Gr.*, Vol.28, No.3, pp.95:1–95:8 (2009).
20) Kang, X., Peng, W., Gabriel, T. and Yu, C.: Blind image restoration using the cepstrum method, *Canadian Conference on Electrical and Computer Engineering*, pp.1952–1955 (2006).
21) Ji, H. and Liu, C.: Motion blur identification from image gradients, *IEEE Conference on Computer Vision and Pattern Recognition*, pp.1–8 (2008).
22) Asai, H., Oyamada, Y., Pilet, J. and Saito, H.: Cepstral analysis based blind deconvolution for motion blur, *IEEE Conference on Image Processing* (2010).
23) Rudin, L., Osher, S. and Fatemi, E.: Nonlinear total variation based noise removal algorithms, Physica D: Nonlinear Phenomena, Vol.60, No.1-4, pp.259–268 (1992).
24) Chan, R.H., Chan, T.F. and Wong, C.-K.: Cosine transform based preconditioners for total variation deblurring, *IEEE Trans. Image Processing*, Vol.8, No.10, pp.1472–1478 (1999).
25) Wang, Y., Yang, J., Yin, W. and Zhang, Y.: A new alternating minimization algorithms for total variation image reconstruction, *SIAM Journal on Imaging Sciences*, Vol.1, pp.248–272 (2008).
26) Cai, J.-F., Ji, H., Liu, C.-Q. and Shen, Z.: Blind motion deblurring from a single image using sparse approximation, *IEEE Conference on Computer Vision and Pattern Recognition* (2009).
27) Vonesch, C. and Unser, M.: A fast multilevel algorithm for wavelet-regularized image restoration, *IEEE Trans. Image Processing*, Vol.18, No.3, pp.509–523 (2009).
28) Richardson, W.H.: Bayesian-based iterative method of image restoration, *Journal of Optical Society of America*, Vol.62, No.1, pp.55–59 (1972).
29) Wiener, N.: Extrapolation, interpolation, and smoothing of stationary time series, *MIT Press* (1964).
30) Levin, A., Sand, P., Cho, T.S., Durand, F. and Freeman, W.T.: Motion-invariant

photography, *ACM Trans. Gr.*, Vol.27, No.3, pp.71:1–71:9 (2008).
31) Whyte, O., Sivic, J., Zisserman, A. and Ponce, J.: Non-uniform deblurring for shaken images, *IEEE Conference on Computer Vision and Pattern Recognition* (2010).
32) Tai, Y.-W., Tan, P., Gao, L. and Brown, M.S.: Richardson-Lucy deblurring for scenes under projective motion path, *IEEE Transactions on Pattern Analysis and Machine Intelligence* (2010).
33) Cho, S., Matsushita, Y. and Lee, S.: Removing non-uniform motion blur from images, *International Conference on Computer Vision* (2007).
34) Joshi, N., Kang, S.B., Zitnick, L. and Szeliski, R.: Image Deblurring using Inertial Measurement Sensors, *ACM Trans. Gr.*, Vol.29, No.4, pp.30:1–30:9 (2010).
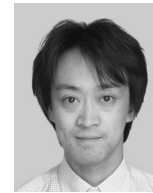
Chika Inoshita received her B.S. degree from Osaka University in 2010. She is a graduate student at Osaka University. She has been engaged in computer vision.

Yasuhiro Mukaigawa received his M.E. and Ph.D. degrees from University of Tsukuba in 1994 and 1997, respectively. He became a research associate at Okayama University in 1997, an assistant professor at University of Tsukuba in 2003, and an associate professor at Osaka University in 2004. His current research interests include photometric analysis and computational photography. He was awarded the MIRU Nagao Award in 2008. He is a member of IEICE, VRSJ, and IEEE.

Yasushi Yagi is a professor at the Institute of Scientific and Industrial Research, Osaka University. He received his Ph.D. degree from Osaka University in 1991. After working at the Product Development Laboratory, Mitsubishi Electric Corporation, he joined Osaka University in 1990. The international conferences for which he served as the program general chair include: ROBIO2006 (PC), ACCV2007 (PC), ACCV2009 (GC) and ACPR2011 (PC). He was the Editor of IEEE ICRA CEB (2008–2011). He is an associate Editor-in-Chief of IPSJ Transactions on CVA. He has received several awards, including the ACM VRST2003 Honorable Mention Award and the PSIVT2010 Best Paper Award. He is a member of IEICE, RSJ, and IEEE.